

# Exploring the Use of GNSS Beyond the Moon

Brian C. Peters, Ryan McKnight, Zachary Arnett, Sabrina Ugazio, Michael Braasch, *Ohio University*

## BIOGRAPHY

**Brian C. Peters** is pursuing his Ph.D. in Electrical Engineering and Computer Science at Ohio University as part of the Avionics Engineering Center. He completed his M.S. in Electrical Engineering at Ohio University in 2021 where he was involved with the development and operation of the Bobcat-1 CubeSat and conducted research on estimation of GNSS inter-constellation time offsets.

**Ryan McKnight** is a Ph.D. candidate at the Avionics Engineering Center, School of Electrical Engineering and Computer Science, Ohio University, where he has worked on PNT research since 2017. His research interests include small satellites, GNSS interoperability, GNSS interference monitoring, weak-signal GNSS, pulsar-based navigation/timing, and deep space navigation. He was previously involved with the development and operations of the Bobcat-1 CubeSat. He received his M.S. in Electrical Engineering from Ohio University in 2023.

**Zachary Arnett** is pursuing his Ph.D. in Electrical Engineering and Computer Science at Ohio University as part of the Avionics Engineering Center. His research interests include GNSS inter-constellation time offset determination and radio-frequency pulsar navigation and timing. He received his B.S. in Electrical Engineering from Ohio University in 2019.

**Sabrina Ugazio** is an Assistant Professor at Ohio University. She obtained her Ph.D. in Electronics and Telecommunications at Politecnico di Torino (Italy) in 2013. Her research interests include timing, remote sensing, GNSS interoperability and space applications.

**Michael Braasch** is the Thomas Professor of Electrical Engineering in the School of EECS at Ohio University. He has been performing navigation research for 37 years and is a Fellow of the Institute of Navigation.

## ABSTRACT

The increasing volume of space missions expected over the coming decades will drive demand for autonomous navigation methods that can reduce reliance on ground-based tracking networks. Past and current research efforts have shown that Global Navigation Satellite Systems (GNSS) can be used to navigate Earth-orbiting spacecraft at high altitudes, above the GNSS constellations themselves, and show great promise as a means of navigating spacecraft in cislunar space and at the Moon. Additional study is required to build on this work and further consider the viability of GNSS-based navigation beyond the Moon. The objective of this paper is to review and analyze current weak-signal GNSS receiver technology for space applications and investigate multi-GNSS signal visibility in specific mission scenarios. It details the design of a simulation considering “L1-band” (L1/E1/B1) and “L5-band” (L5/E5a/L3/B2) signals from GPS, Galileo, GLONASS, BeiDou, QZSS, and NavIC, evaluating expected visibility from main lobe and sidelobe signals using estimated antenna patterns. Results from the simulation are shown for three specific scenarios: a straight-line trajectory from 60 Earth radii (RE) (approximate lunar distance) to 300 RE covering 14 days, 7 days surrounding the apogee of NASA’s Cislunar Autonomous Positioning System Technology Operations and Navigation Experiment (CAPSTONE) during its ballistic lunar transfer (BLT), and the final 7 days of NASA’s Double Asteroid Redirection Test (DART) mission before impact with the asteroid Dimorphos.

## I. INTRODUCTION

The coming decades are expected to see a substantial increase in the number of missions to the Moon and beyond (Cohen et al., 2021; Turan et al., 2022). This has inspired numerous research efforts to identify low-cost methods for autonomous navigation of spacecraft beyond Earth that can reduce the amount of ground-based tracking required by systems such as NASA’s Deep Space Network (DSN). Radiometric data produced by ground tracking networks has long been the predominant method for navigating spacecraft in deep space. Spacecraft tracking networks typically provide range and Doppler data, which are recorded over a span of hours and post-processed to estimate the trajectory of a spacecraft. The DSN is currently used to operate numerous missions in deep space and at the Moon. For many missions, the cost of utilizing the DSN can be prohibitive with the need for observations to be scheduled on a limited number of ground stations which are routinely oversubscribed (Johnston, 2020). Autonomous or semi-autonomous navigation methods that can reduce the need for scheduled observations with the DSN can therefore be highly beneficial and serve to reduce the operational complexity and cost of deep space navigation.

Previous research efforts have sought to determine the viability of autonomous navigation of spacecraft in cislunar space using Earth-centric Global Navigation Satellite Systems (GNSS) (Bauer et al., 1998; Braasch & Uijt de Haag, 2006; Ashman et al.,

2018; Delépaut et al., 2020). Notably, NASA's Magnetic Multiscale (MMS) mission has demonstrated operational use of GPS at 29 Earth radii (RE), nearly half the distance to the Moon, using NASA's high-heritage Navigator receiver (Parker et al., 2022; Winternitz, Bamford, & Price, 2017). A case study comparing DSN and GPS-based navigation for NASA's planned lunar Gateway station conducted by Winternitz et al. (2019) suggests that GPS may also be able to provide autonomous navigation capability that meets or exceeds the performance of the DSN for the Gateway's near-rectilinear halo orbit (NRHO). These encouraging results have inspired projects such as the Lunar GNSS Receiver Experiment (LuGRE), which aims to demonstrate the use of GNSS on and near the Moon using a QN400 GPS/Galileo receiver developed by Qascom (Parker et al., 2022), and the European Space Agency's (ESA's) Lunar Pathfinder mission, which will utilize a NAVIMOON GPS/Galileo receiver developed by SpacePNT (Pultarova, 2022). Several recent investigations have also explored the use of Earth-GNSS to localize navigation/communications satellites operating at the Moon to provide dedicated lunar position, navigation, and timing (PNT) services (Small et al., 2022; Bhamidipati et al., 2023). NASA's LunaNet (Israel et al., 2020) and ESA's Moonlight initiative (Cozzens, 2021) aim to realize PNT and communications services for lunar end users, enabled by relay satellites equipped with high-sensitivity GNSS receivers. Although a great deal of focus has recently been placed on the applicability of GNSS navigation for lunar users, few studies have speculated on the utility or feasibility of GNSS-based navigation beyond cislunar space.

Methods for high-altitude GNSS navigation that have been demonstrated by missions such as MMS have clearly established that GNSS can be a viable method for spacecraft navigation beyond medium Earth orbit (MEO), above the GNSS constellations themselves. These successes have largely been driven by advanced high-sensitivity receiver architectures that allow for acquisition and tracking of very low carrier-to-noise ratio signals received mainly from the sidelobes of GPS antenna patterns (Winternitz, Bamford, & Price, 2017). The higher gain of the main lobe signals provides a clear advantage in terms of link margin for acquisition, though these signals are less often visible at high altitudes. Delépaut et al., 2020 characterizes the number of visible signals from GPS and Galileo main lobes and sidelobes for a receiver in NRHO, enabled by accurate transmit antenna patterns of GPS satellites provided in Marquis and Reigh (2015) and Donaldson et al. (2020), and internally-sourced data for Galileo. This analysis found that less than 20% of received signals were from main lobe transmissions for both the L1 and L5 bands. Studies that consider the potential of a fully interoperable GNSS space service volume (SSV), such as Parker et al., 2018; Enderle et al., 2018; Ugazio et al., 2020 have shown strong visibility of main lobe signals when combining all available constellations, with 4 or more signals visible nearly 100% of the time throughout the high-altitude SSV. These analyses also highlight the significant visibility improvement provided by signals in the L5 frequency band.

A software receiver architecture for lunar missions described in Musumeci et al. (2016) demonstrated GPS (L1/L5) and Galileo (E1/E5) signal acquisition at carrier-to-noise ratios as low as 8 dB Hz using external data aiding and orbital filter coupling. Blunt et al. (2016) describes the Spaceborne Autonomous Navigation based on GNSS (SANAG) GPS/Galileo receiver which is capable of 15 dB Hz acquisition with orbital filter aiding and no assistance data. This weak signal tracking capability can be leveraged to perform trajectory estimation autonomously using recorded range and Doppler measurements even when point solutions cannot be computed. Deep space trajectories often contain extended periods of time with minimal acceleration, providing a low-dynamic environment that can facilitate long integration and lower acquisition thresholds when aided by an onboard navigation filter with an a priori trajectory estimate. With adequate GNSS visibility, a multi-GNSS receiver can leverage advanced weak-signal acquisition and tracking techniques with high-gain, low-noise RF front-ends to reduce or eliminate the current dependency on DSN tracking for navigation beyond lunar distances.

Past research efforts have shown that GNSS can be used to navigate Earth-orbiting spacecraft at altitudes above the GNSS constellations themselves and more recent studies conclude that GNSS shows great promise as a means of navigating spacecraft at the Moon. Further analysis is required to build on this work and consider the viability of GNSS-based navigation beyond lunar distances. The objective of this paper is to explore possible mission concepts that may benefit from the use of GNSS and evaluate GNSS signal visibility in these scenarios. High-altitude weak-signal GNSS receiver architectures, processing techniques, and published results from past GNSS experiments are discussed. The role that GNSS-based navigation can fill in realistic mission scenarios such as ballistic lunar transfers or near-Earth asteroid missions is explored along with the receiver capabilities required for these missions. Multi-GNSS system coverage beyond the Moon is characterized using results from a simulation developed using signals from GPS, Galileo, GLONASS, BeiDou, QZSS, and NavIC.

## II. BACKGROUND

### 1. Deep Space Navigation

Traditionally, ground-based radiometric tracking through systems such as the DSN have formed the basis for telecommand and navigation of spacecraft in deep space. Most commonly, two-way radiometric range and Doppler measurements are recorded over the span of a few hours and used to form trajectory estimates. Two-way range and Doppler measurements made by the DSN are highly precise, typically achieving 1 to 3 m  $1\sigma$  range error and  $< 0.1$  mm/s  $1\sigma$  range rate error (Ely et al., 2022). Since the 2000's, the DSN has also employed delta differential one-way range ( $\Delta$ DOR) measurements (*DSN Telecommunications Link Design Handbook*, 2018) that can provide information about a spacecraft's angular location relative to a reference object with known direction of arrival ( $1\sigma$  error of 2-3 nanoradians).  $\Delta$ DOR measurements are complementary to two-way range and

Doppler measurements and improve the overall navigation performance, but require the use of two ground stations at once.

Though it is difficult to generalize the cost of using the DSN, since prices are ultimately driven by the navigation requirements and specific services needed over the course of a mission, the total cost per year can easily reach into the millions of dollars. The base hourly rates for DSN single spacecraft tracking are provided in *Space Communications and Navigation (SCaN) Mission Operations and Communications Services (MOCS)* (2021) and shown in Table 1.

**Table 1:** Base rates for DSN single spacecraft tracking (FY2021)

Station	Hourly Rate
Single 34-m Station	\$1792 per hour
Two 34-m Array	\$3583 per hour
Three 34-m Array	\$5375 per hour
Four 34-m Array	\$7167 per hour
70-m Stations	\$5375 per hour

NASA provides an online tool (“DSN Aperture Fee Calculator,” 2022) that can be used to more accurately estimate DSN costs, accounting for setup and teardown and additional cost multipliers associated with the specific DSN activities required by a mission. An example mission is provided in the aperture fee calculator (MSNX2020), which shows the cost breakdown for 3 years of DSN support. The total cost (assuming FY2017 rates) comes to \$10,240,180, with over \$6,000,000 of the total cost incurred during the first year of the mission. Though the dependence on ground networks for telecommand cannot be eliminated, reducing tracking time required to meet mission navigation requirements can still stand to greatly reduce costs.

Studies conducted by Winternitz et al. (2019) and Small et al. (2022) suggest that GPS-based navigation with a highly-stable onboard clock may be able to achieve navigation performance for lunar spacecraft that exceeds the performance achievable with ground-based tracking. Winternitz et al. (2019) additionally shows that error scaling differs for two-way and one-way radiometric systems, where one-way ranging errors grow more rapidly than two-way with distance due to the dependence on the local clock. The incredibly high ( $>1000$ ) geometric dilution of precision (GDOP) at lunar distances limits navigation accuracy attainable with single-epoch least-squares GNSS point solutions. This necessitates the use of onboard navigation filters and highly-stable clocks, especially for spacecraft at even greater distances.

## 2. Weak-Signal GNSS Receivers for Spacecraft

A significant amount of research and development effort has been directed toward GNSS-based navigation beyond MEO, and much of this work has been in pursuit of GNSS receivers capable of operating at lunar distances. Such lunar GNSS receivers must be capable of acquiring and tracking very low carrier-to-noise ratio ( $C/N_0$ ) signals and must tolerate much larger Doppler shifts and Doppler rates than are common for Earth receivers (Capuano et al., 2017). NASA’s Navigator receiver described in Winternitz et al. (2004) currently holds the record for the highest-altitude GPS fix, and is an example of a fully-autonomous receiver architecture. That is to say, a design principle of Navigator is that it does not depend on any external data aiding or a converged filter estimate of the receiver dynamics. Navigator’s orbital filter, called the Goddard Enhanced Onboard Navigation System (GEONS) is not used to aid signal acquisition. Receiver designs considered in Musumeci et al. (2016), Blunt et al. (2016), and Capuano et al. (2017) employ various methods for aided signal acquisition. Common to nearly all existing and proposed spaceborne weak-signal GNSS receiver architectures is the reliance on orbital navigation filters, since there are often too few tracked signals to compute point solutions and acquisition can be significantly improved using advanced filter-aiding methods.

Winternitz et al. (2004) details the design of the first version of the Navigator receiver. Navigator has earned significant flight heritage and has demonstrated acquisition and tracking of GPS L1 C/A signals at a  $C/N_0$  of 25 dB Hz. Navigator, like most other high-sensitivity receivers, applies a parallel/batch processing approach to signal acquisition. In its weak signal mode, the receiver collects consecutive 10 ms correlations. The set of these correlations that is free of data bit transitions can then be combined non-coherently by taking the magnitude squared and summing over some desired quantity, following the “half-bits” method described in Psiaki (2001). After a successful detection, the receiver initializes a standard FLL/PLL/DLL-based tracking channel with the estimated Doppler shift and delay. In Winternitz, Bamford, Price, et al. (2017) and Winternitz, Bamford, and Price (2017) navigation results from Navigator aboard MMS are analyzed, showing that point solutions were frequently available at 25 RE. On average, three signals were tracked near apogee with a maximum of 8 recorded. The authors noted that the majority of tracked signals were received from transmitter sidelobes. MMS flew a configuration of four GPS antennas around the spacecraft perimeter, each with 4 dBi gain. Work is currently underway at NASA Goddard Space Flight Center on new versions of Navigator which can support modernized GPS signals and other GNSS constellations (Petrick et al., 2015).

Capuano et al. (2017) and Blunt et al. (2016) describe two receivers, WeakHEO and the SANAG receiver, built by the Electronics

and Signal Processing Laboratory (ESPLAB) at Ecole Polytechnique Fédérale de Lausanne (EPFL). WeakHEO was built as a proof of concept for a GNSS signal processing engine for lunar mission scenarios, from which SANAG was developed as a follow-on. SANAG is a dual frequency L1/E1, L5/E5 receiver capable of unaided acquisition at 18 dB Hz and orbital filter-aided acquisition at 15 dB Hz with a minimum tracking sensitivity of 12 dB Hz. A notable difference between the SANAG and Navigator receivers is the use of frequency and frequency-rate aiding from the orbital filter, which reduces both the minimum acquisition threshold and processing time required.

Musumeci et al. (2016) presents the design of a high-sensitivity GPS/Galileo receiver architecture for lunar missions, and conducts a detailed analysis of its simulated performance throughout all phases of a realistic lunar mission (using the European Space Agency’s Lunar Lander mission as a reference), from launch through highly dynamic maneuvers and descent to the lunar surface and surface operations. The receiver architecture considered in this study implements GPS L1/L5 and Galileo E1/E5a, and is designed to achieve 8 dB Hz acquisition and 5 dB Hz tracking using very long coherent integration ( $>1$  s). In addition to a highly accurate and tightly-coupled orbital filter, this architecture employs assistance data (which could be assumed to be provided by a low data rate link) to allow wipeoff of data bits for longer coherent integration and to reduce the Doppler search space domain for acquisition by centering the search space on the expected Doppler of a given satellite. This receiver, Navigator, and SANAG form the basis for the assumptions of user receiver performance in the simulation of GNSS visibility described in the following section.

### III. SIMULATION DESIGN

A GNSS visibility analysis was conducted using a simulation written in MATLAB. The configurations of each GNSS constellation as of May 18, 2023 were used, and are summarized in Table 2. For simplicity, this simulation only considers signals broadcast in the L1 and L5 bands following from past analyses and simulations of high-altitude GNSS availability (Parker et al., 2018; Enderle et al., 2018). The number of space vehicles (SVs) transmitting in each band is also shown in Table 2, and is configured to match the actual operational constellations. Table 3 summarizes the RF parameters assigned to each group of GNSS satellites used in the simulation.

**Table 2:** GNSS Constellation Details

System	Number of SVs	Frequencies	Semi-major axis (km)	Inclination (°)
GPS	MEO: 31	L1: 31 SVs L5: 17 SVs	26 560	55
GLONASS	MEO: 24	L1: 24 SVs L3: 9 SVs	25 510	64.8
Galileo	MEO: 23	E1: 23 SVs E5a: 23 SVs	29 600	56
BDS	MEO: 27 GEO: 7 IGSO <sup>1</sup> : 10	B1: 44 SVs B2: 42 SVs	27 906 42 164 42 164	55 0 55
QZSS	QZO <sup>2</sup> : 3 GEO: 1	L1: 4 SVs L5: 4 SVs	42 164 42 164	43 0
NavIC	GEO: 3 IGSO <sup>1</sup> : 4	L5: 7 SVs	42 164 42 164	0 29

<sup>1</sup> inclined geosynchronous orbit (IGSO)

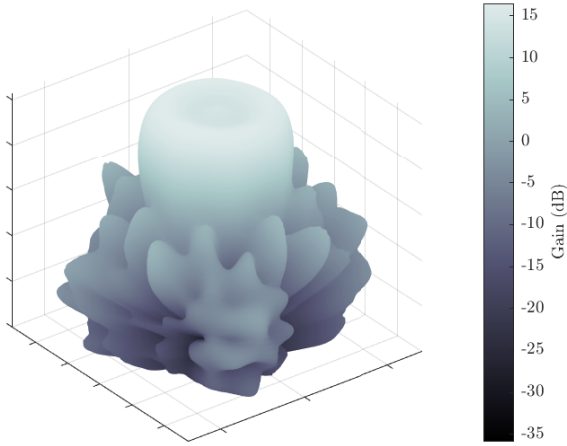
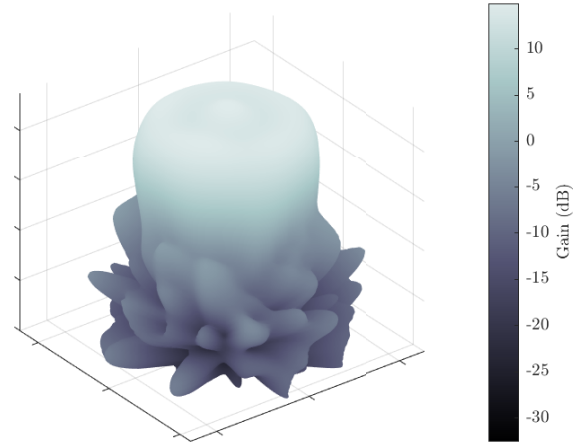
<sup>2</sup> quasi-zenith orbit (QZO)

This simulation uses scaled GPS Block III antenna patterns (shown in figures 1, 2 and 3) for all SVs (United States Coast Guard Navigation Center, n.d.). The patterns are scaled by computing the difference between the main beamwidth of the GPS Block III pattern and the main beamwidth corresponding to a given SV according to Table 3. This difference is applied as an offset to the off-boresight angle of the GPS Block III antenna pattern. It should be noted that the axial ratio of high off-boresight angle signals is generally not well-known, and there could be additional loss due to polarization mismatch in signals received from the sidelobes.

In this simulation, the yaw angle of each GNSS satellite about its antenna boresight is fixed to an arbitrary value. In practice, this angle varies with time in a defined manner which can affect the observed signal strength due to azimuthal variations in the antenna pattern (Montenbruck et al., 2015). For the purposes of this simulation, which only considers visibility statistics, the

**Table 3:** GNSS Constellation Information (United Nations Office for Outer Space Affairs, 2021)

GNSS constellation	Signal	Frequency (MHz)	Max beamwidth (°)	Transmit power (dBW)
GPS	L1 C/A	1575.42	23.5	9.1
GPS	L5	1176.45	26	8.5
Galileo	E1 B/C	1575.42	20.5	10.9
Galileo	E5a	1176.45	23.5	8.5
BDS MEO	B1	1575.42	25	9.0
BDS GEO-IGSO	B1	1575.42	19	9.0
BDS MEO	B2	1191.795	28	8.0
BDS GEO-IGSO	B2	1191.795	22	8.1
GLONASS	L1	1605.375	20	14.1
GLONASS	L3	1201	28	12.6
QZSS	L1 C/A	1575.42	22	9.0
QZSS	L5	1176.45	24	9.2
NavIC	L5	1176.45	16	7.8

**Figure 1:** Average GPS Block III L1 antenna pattern**Figure 2:** Average GPS Block III L5 antenna pattern

effect is expected to be minimal (Shehaj et al., 2017).

Three separate scenarios were evaluated and are summarized in Table 4. Case 1 applies user receiver specifications previously considered by Winternitz, Bamford, and Price (2017) and inspired by NASA’s Navigator. The user is defined as moving in a straight line directly out of the x axis of an Earth-centered inertial frame between 60 RE (approximate lunar distance) and 300 RE over a time span of 14 days, using 2 minute time steps. This first case is intended to illustrate the maximum distance at which a Navigator-like receiver platform could be capable of acquiring signals. Cases 2 and 3 represent recent NASA missions which traveled beyond the Moon and utilize ephemerides retrieved from NASA’s Horizons system (Jet Propulsion Laboratory, 2023). Case 2 simulates 7 days (at 1 minute intervals) surrounding the apogee of NASA’s Cislunar Autonomous Positioning System Technology Operations and Navigation Experiment (CAPSTONE) (Cheetham, 2021), which used a ballistic lunar transfer (BLT) to enter a NRHO in November, 2022 (Wall, 2022). CAPSTONE’s ballistic lunar transfer reached an apogee of  $\sim 1.5$  million km. Case 3 applies the highest performance specifications to the user, and simulates the last 7 days (at 1 minute intervals) of NASA’s Double Asteroid Redirection Test (DART) mission before impact with asteroid Dimorphos  $\sim 11.3$  million km from Earth in September, 2022. The user’s antenna gain is set to 24 dB in Case 3, which is approximately equivalent to a 1.5 m dish.

The user’s system noise temperature,  $T_{sys}$  is constant in all scenarios and is defined as  $T_{sys} = 290 \text{ K} \times 10^{\text{NF}/10-1} + T_{ant}$  where the noise figure (NF) is assumed to be 1 dB and  $T_{ant}$  is 100 K, resulting in a  $T_{sys}$  of 175 K. This assumption implies a high-performance RF front-end with a very low-noise amplifier and low insertion loss filter.

At each time step, the simulation determines line-of-sight visibility between the user all GNSS SVs assuming a 50 km atmospheric

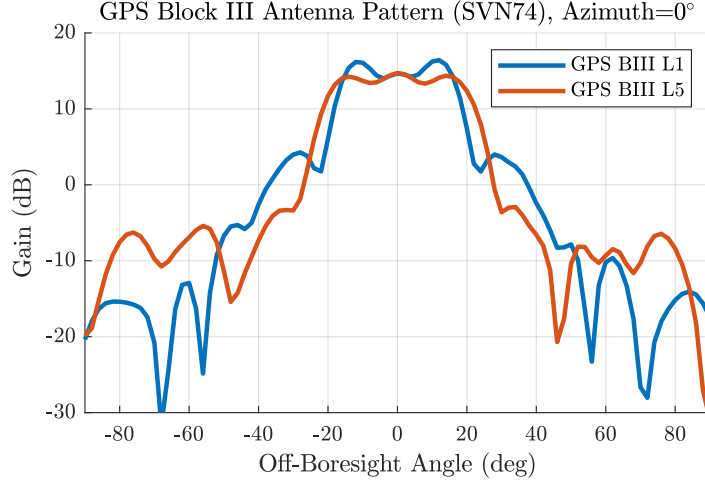


**Figure 3:** Azimuth cut of GPS SVN74 antenna patterns

mask and maximum off-boresight angle of  $80^\circ$  (to avoid signals that interfere with the GNSS satellite body). The received power and carrier-to-noise-density ratio are then computed for each visible L1-band and L5-band signal at each time step using the following equations:

$$P_r = P_t + G_t(\theta, \phi) + G_r + \underbrace{20 \log_{10} \left( \frac{\lambda}{4\pi R} \right)}_{L_{fs}} \quad (1)$$

$$C/N_0 = P_r - 10 \log_{10}(kT_{sys}) \quad (2)$$

Where:

$P_r$  is the received power (dBW)

$P_t$  is the SV's antenna input power, retrieved from Table 3 for each SV (dBW)

$G_t$  is the gain of the SV antenna (dB), which is a function of elevation  $\theta$  and azimuth  $\phi$

$G_r$  is the gain of the receiver antenna (dB)

$\lambda$  is the signal wavelength (m)

$R$  is the distance (m)

$L_{fs}$  is the free-space loss term, which varies as a function of distance (dB)

$C/N_0$  is the received carrier-to-noise-density ratio (dBHz)

$T_{sys}$  is the user's system noise temperature (K)

$k$  is Boltzmann's constant (J/K)

**Table 4:** Simulation Scenarios

Scenario	Trajectory	Dates	Acq. Threshold (dB-Hz)	Antenna Gain (dB)
Case 1	Straight line, 60 RE to 300 RE	2022-03-20 to 2022-04-03	25	14
Case 2	CAPSTONE	2022-08-23 to 2022-08-30	15	14
Case 3	DART	2022-09-19 to 2022-09-26	8	24

## IV. RESULTS

### 1. Case 1

Signal visibility for Case 1 is shown in Figure 4 and Figure 5 shows the altitude of the receiver throughout the simulation. It is observed that L5-band signal visibility is significantly better than the L1-band, despite there being fewer satellites transmitting in the L5 band. No L1-band signals are visible beyond 1 million km, while in L5 there is limited visibility up to nearly 1.5 million km.

Figures 6 and 7 show the  $C/N_0$  at the receiver from all signals over the first 24 hours of the simulation. In these plots the stronger but less frequent main lobe signals can be seen rising above the dense collection of sidelobe signals. For the L1 band, the majority of these sidelobe signals fall just below the Case 1 receiver threshold of 25 dB-Hz in Figure 6. In the GPS Block III patterns used for this simulation, the gain of the first sidelobe is considerably lower in L5 than L1. This lower sidelobe gain is apparent in Figure 7. Figures 8 and 9 illustrate that nearly all signals received beyond the Moon with this specific user receiver configuration are from main lobe transmissions.

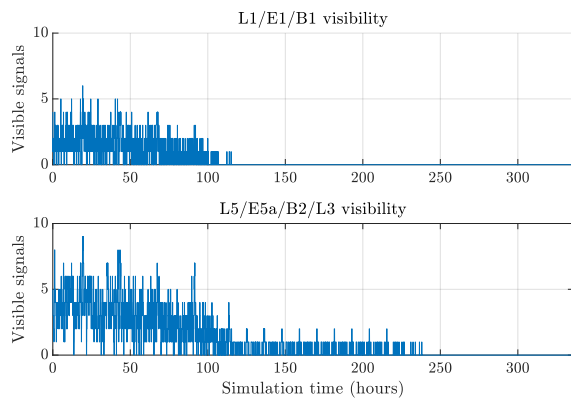


Figure 4: Case 1 overall signal visibility.

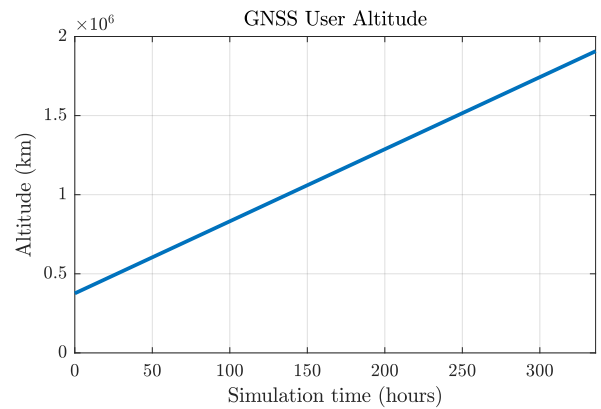


Figure 5: Case 1 user altitude.

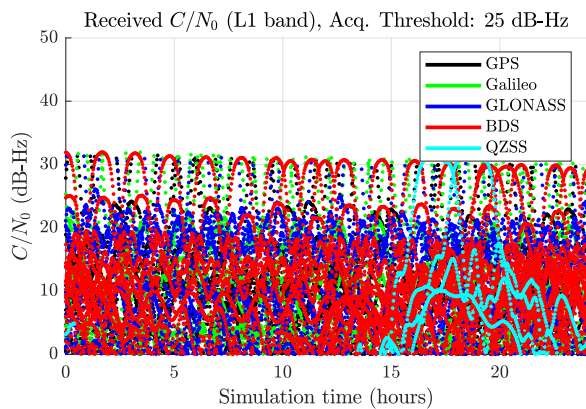


Figure 6: Case 1 L1-band  $C/N_0$ .

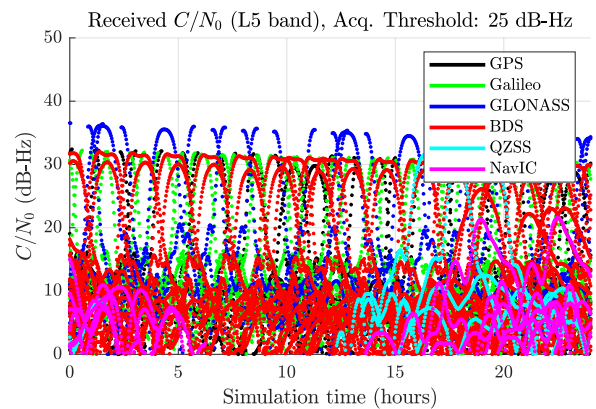
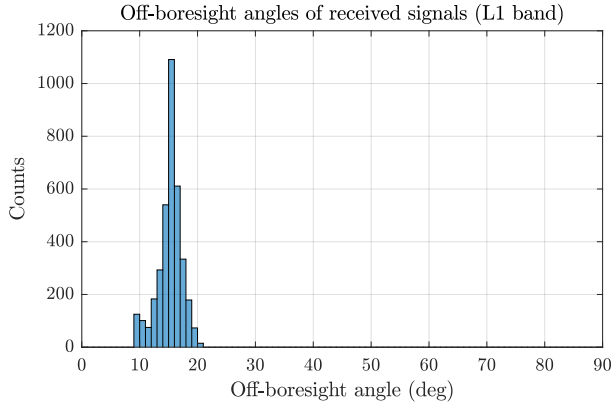
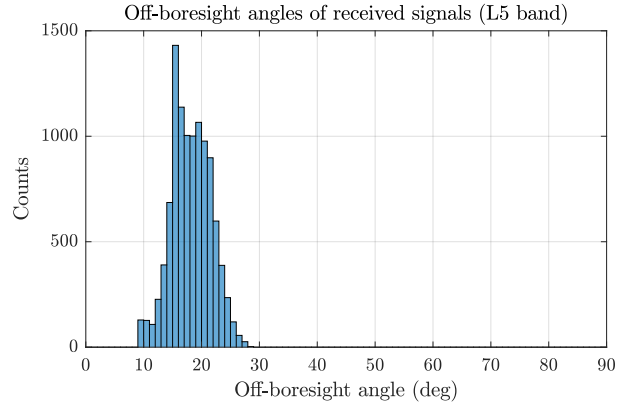


Figure 7: Case 1 L5-band  $C/N_0$ .



**Figure 8:** Case 1 L1-band off-boresight angle histogram.



**Figure 9:** Case 1 L5-band off-boresight angle histogram.

## 2. Case 2

Case 2 highlights a particularly compelling use-case of GNSS signals beyond lunar distances, where spacecraft employing high-efficiency/high-altitude lunar transfers could potentially rely on GNSS-based navigation throughout the entire mission. These spacecraft could utilize GNSS signals during the transfer and after reaching orbit at the Moon. Figure 10 shows the total number of visible signals in each band over time, again with greater visibility in the L5 band. Figure 11 shows the altitude of the user through the apogee of CAPSTONE's BLT. Periodic spikes in visibility are observed every 24 hours in Figure 10, attributable to the larger number of geosynchronous satellites over Earth's eastern hemisphere.

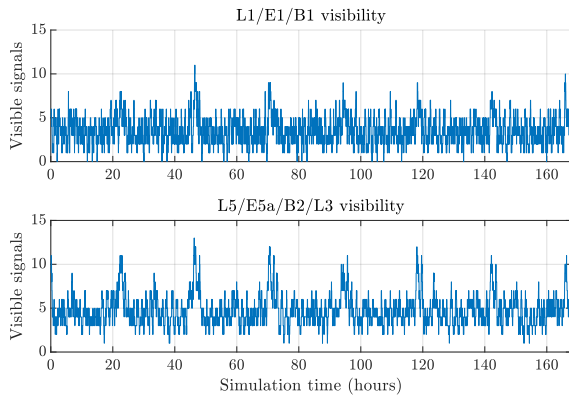


**Figure 10:** Case 2 overall signal visibility.

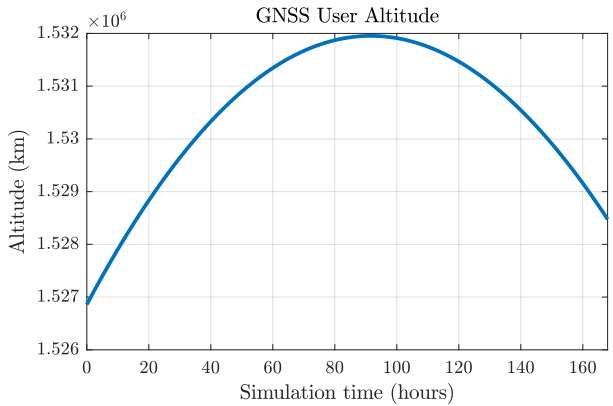


**Figure 11:** Case 2 user altitude (CAPSTONE BLT).

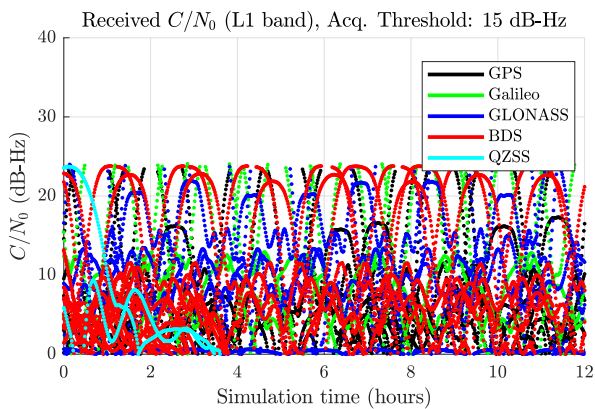


**Figure 12:** Case 2 L1-band  $C/N_0$ , first 12 hours of simulation.

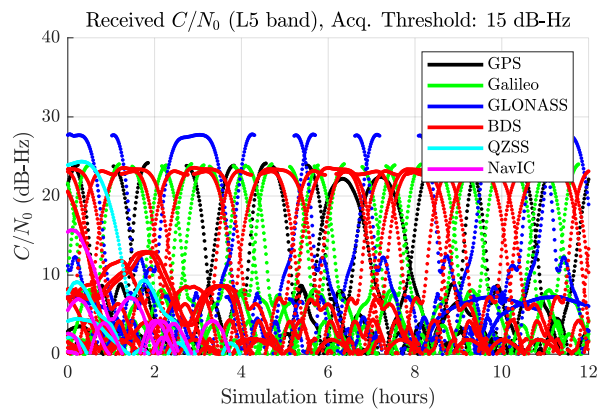


**Figure 13:** Case 2 L5-band  $C/N_0$ , first 12 hours of simulation.

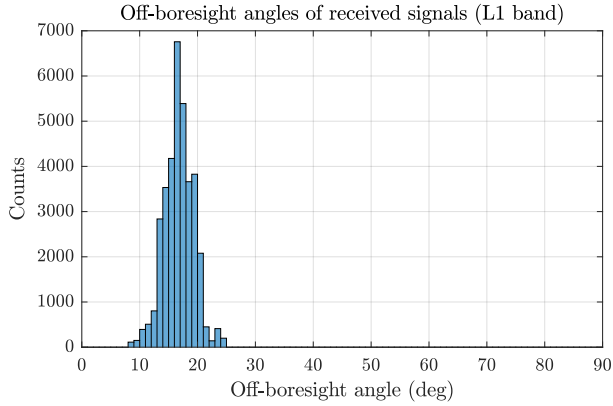


**Figure 14:** Case 2 L1-band off-boresight angle histogram.

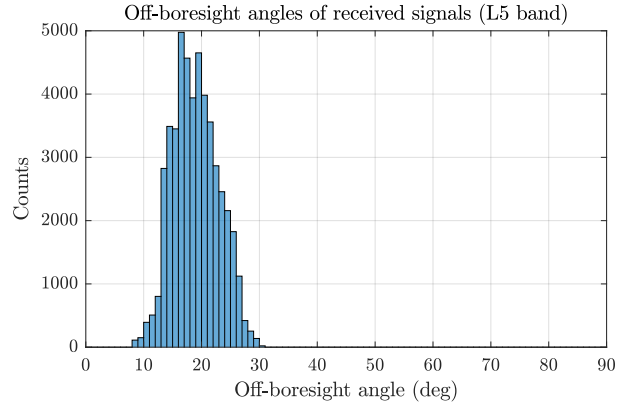


**Figure 15:** Case 2 L5-band off-boresight angle histogram.

As shown in Table 5, at least one signal is visible nearly 100% of the time for both the L1 and L5 bands when combining all constellations. The average track length and maximum outage durations (MODs) for  $\geq 1$  and  $\geq 4$  signals are shown for both bands. BeiDou is shown to be the only individual constellation capable of achieving  $\geq 4$  signal coverage at any point on its own, due to BeiDou having more operational satellites than any other system (44 total in this simulation).

**Table 5:** Case 2 visibility statistics.

Band	Constellation	Avg. track len. (min)	At least 1 signal		4 or more signals	
			Avail. (%)	MOD (min)	Avail. (%)	MOD (min)
L1/E1/B1	GPS	16.2	53.2	2580.0	0.0	-
	Galileo	12.3	39.9	3420.0	0.0	-
	GLONASS	12.8	62.4	2400.0	0.0	-
	BeiDou	44.2	92.3	840.0	2.8	84 420.0
	QZSS	50.0	11.7	70 500.0	0.0	-
	<b>Combined</b>	-	-	99.4	540.0	47.1
L5/E5a/L3/B2	GPS	28.3	57.8	3120.0	0.0	-
	Galileo	23.4	75.2	2640.0	0.0	-
	GLONASS	35.1	53.9	3240.0	0.0	-
	BeiDou	65.4	100.0	0.0	12.1	40 380.0
	QZSS	71.9	18.1	67 920.0	0.0	-
	NavIC	19.4	2.9	81 480.0	0.0	-
<b>Combined</b>	-	-	100.0	0.0	79.1	3300.0

### 3. Case 3

In Case 3, similar visibility statistics are observed to those in Case 2. The user's receiver configuration has an additional 17 dB of sensitivity over that of Case 2 (+10 dB of antenna gain and +7 dBHz of receiver sensitivity), and the distances considered here result in  $\sim 18$  dB additional free-space path loss over Case 2. Figures 16, 17, 18, 19, 20, and 21 illustrate the Case 3 results and Table 6 summarizes the overall visibility statistics. Case 3 results suggest that this user configuration could likely acquire and track signals at even greater distances as figures 18 and 19 indicate considerable margin between the 8 dBHz receiver threshold and the strongest main lobe signals.

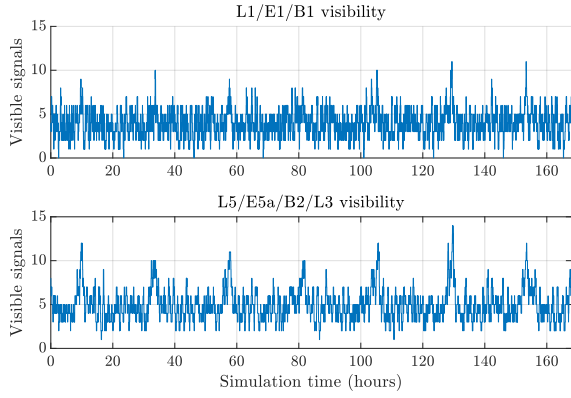


**Figure 16:** Case 3 overall signal visibility.

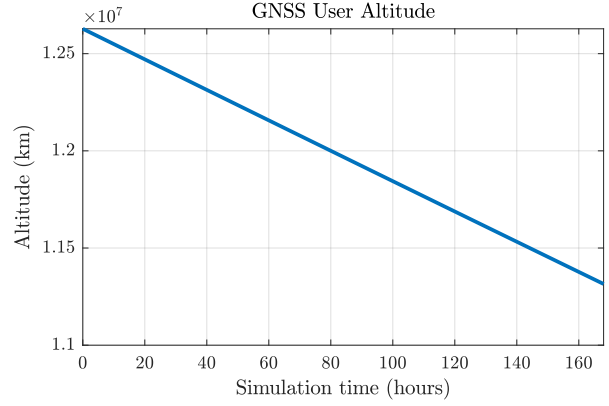


**Figure 17:** Case 3 user altitude.

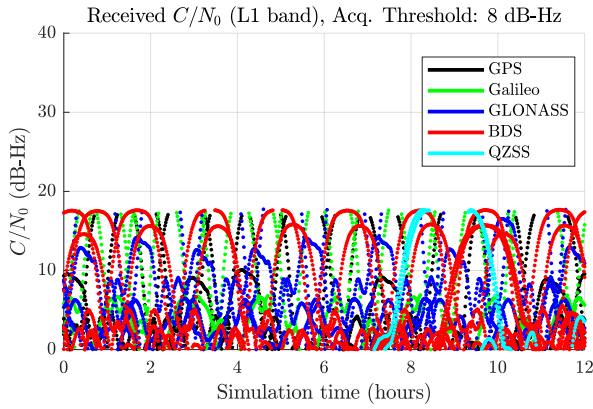


**Figure 18:** Case 3 L1-band  $C/N_0$ , first 12 hours of simulation.

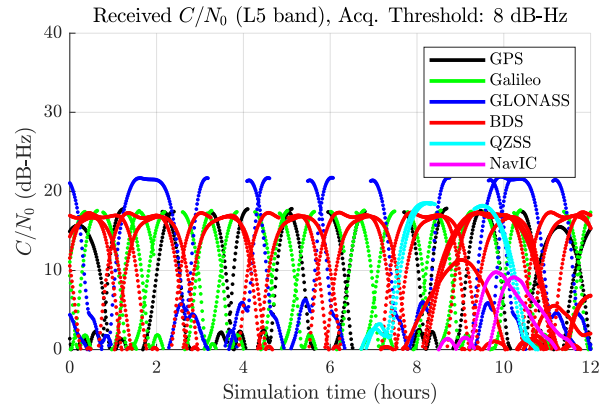


**Figure 19:** Case 3 L5-band  $C/N_0$ , first 12 hours of simulation.

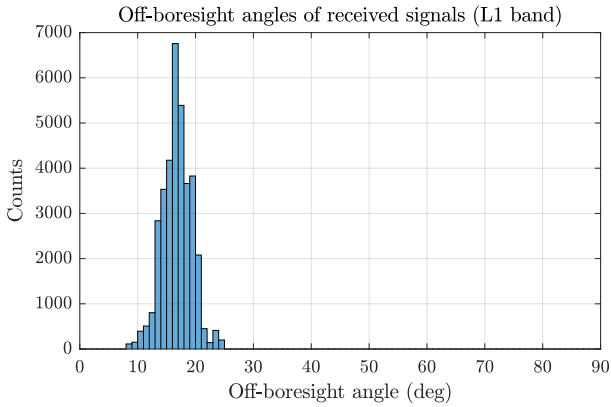


**Figure 20:** Case 3 L1-band off-boresight angle histogram.

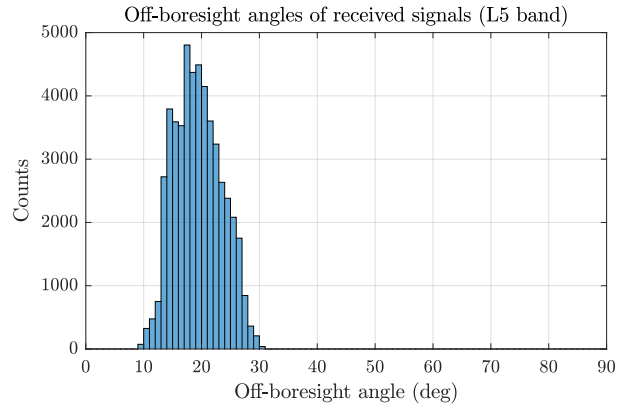


**Figure 21:** Case 3 L5-band off-boresight angle histogram.

**Table 6:** Case 3 visibility statistics.

Band	Constellation	Avg. track len. (min)	At least 1 signal		4 or more signals	
			Avail. (%)	MOD (min)	Avail. (%)	MOD (min)
L1/E1/B1	GPS	17.7	56.4	2580.0	0.0	-
	Galileo	13.0	41.8	3420.0	0.0	-
	GLONASS	17.2	76.6	1500.0	0.0	-
	BeiDou	61.5	93.0	900.0	3.3	83 340.0
	QZSS	38.0	5.7	78 060.0	0.0	-
	<b>Combined</b>	-	-	99.8	300.0	60.2
L5/E5a/L3/B2	GPS	30.2	60.7	3180.0	0.0	-
	Galileo	23.2	73.2	2760.0	0.0	-
	GLONASS	39.5	55.1	3240.0	0.0	-
	BeiDou	88.5	100.0	0.0	13.5	40 320.0
	QZSS	54.9	8.2	75 900.0	0.0	-
	NavIC	36.9	3.8	82 920.0	0.0	-
<b>Combined</b>	-	-	100.0	0.0	80.6	2880.0

Across all three cases shown here it is observed that L5-band visibility is better than the L1-band, despite the fact that the L5-band signals are mostly assigned lower transmit power (Table 3) and fewer satellites transmit these signals. The off-boresight angle histograms illustrate that this is due to the larger main beamwidths in the L5 band. These results assume the same threshold for both acquisition and tracking. Since in practice most receivers are capable of tracking signals at a lower  $C/N_0$  threshold, the visibility statistics produced by the simulation and shown here could be considered conservative.

## V. CONCLUSIONS

In this work, multi-GNSS signal visibility was examined for three specific scenarios beyond lunar distances. In all three cases, it was observed that main lobe signals were most prevalent. These results suggest that existing receiver architectures could be capable of tracking GNSS signals far beyond the Moon, with  $12.6 \times 10^6$  km being the farthest distance considered in this work. The higher gain of main lobe transmissions received across Earth's limb extends the maximum distance at which GNSS signals can be received, though they are typically in view of high-altitude space users for shorter durations when compared with sidelobe signals. Multi-GNSS receiver capability is shown to significantly enhance GNSS visibility. Sidelobe signals are within reach of current spaceborne GNSS receivers at lunar distances, as shown by several previous analyses, but receivers with similar sensitivity would need to rely on main lobe signals for the extralunar distances considered in this simulation.

This simulation does not consider realistic attitude dynamics of GNSS satellites, which significantly affects the observed transmitter gain as sidelobe signals are irregular in azimuth. Additionally, the method of applying elevation offsets to GPS Block III antenna patterns used in this work is also likely to distort the actual gain of sidelobes at a specific off-boresight angle. The effects of these assumptions are believed to be minimal in these results, since sidelobe reception was rare at the distances considered here.

Future work will involve extending this simulation to survey a larger volume of points in space to more clearly define ranges at which specific GNSS receiver configurations could operate. Another topic of future study is to perform more detailed modeling of GNSS signal reception at these distances to ultimately estimate measurement error and navigation performance that could be achieved. Investigation of navigation filters and processing techniques must be conducted to determine how GNSS measurements could most effectively be used to navigate spacecraft in deep space.

## ACKNOWLEDGMENTS

This work was supported by Ohio University. The authors would like to thank Dr. Frank van Graas, Dr. Ben Ashman, and Dr. Luke Winternitz for their advice and insights which helped guide the development of this simulation.

## REFERENCES

- Ashman, B. W., Parker, J. J. K., Bauer, F. H., & Esswein, M. (2018). Exploring the limits of high altitude GPS for future lunar missions [AAS 18-082]. *Proceedings of the 41st Annual AAS Rocky Mountain Section Guidance and Control Conference (AAS/GNC 2018)*.
- Bauer, F. H., Hartman, K., & Lightsey, E. G. (1998). Spaceborne GPS current status and future visions. *1998 IEEE Aerospace Conference Proceedings (Cat. No.98TH8339)*, 3, 195–208. <https://doi.org/10.1109/AERO.1998.685798>
- Bhamidipati, S., Mina, T., & Gao, G. (2023). A case study analysis for designing a lunar navigation satellite system with time transfer from the earth GPS. *NAVIGATION: Journal of the Institute of Navigation*, 70(4). <https://doi.org/https://doi.org/10.33012/navi.599>
- Blunt, P., Botteron, C., Capuano, V., Ghamari, S., Rico, M., & Farine, P.-A. (2016). Ultra-high sensitivity state-of-the-art receiver for space applications. *ESA Workshop on Satellite Navigation Technologies and European Workshop on GNSS Signals and Signal Processing (NAVITEC)*.
- Braasch, M. S., & Uijt de Haag, M. (2006). GNSS for LEO, GEO, HEO and beyond [AAS 06-041]. *Proceedings of the 29th Annual AAS Rocky Mountain Guidance and Control Conference (AAS/GNC 2006)*, 165–194.
- Capuano, V., Blunt, P., Botteron, C., & Farine, P.-A. (2017). Orbital filter aiding of a high sensitivity GPS receiver for lunar missions. *NAVIGATION: Journal of the Institute of Navigation*, 64(3), 323–338. <https://doi.org/10.1002/navi.185>
- Cheetham, B. (2021). Cislunar autonomous positioning system technology operations and navigation experiment (CAPSTONE) [AIAA 2021-4128]. *ASCEND 2021*. <https://doi.org/10.2514/6.2021-4128>
- Cohen, B., Lawrence, S., Denevi, B., Glotch, T., Hurley, D., Neal, C. R., Robinson, M., Watkins, R., & Weber, R. (2021). Lunar missions for the decade 2023-2033. *Bulletin of the AAS*, 53(4). <https://doi.org/10.3847/25c2cfcb.7caeba4e>
- Cozzens, T. (2021). Galileo will help lunar pathfinder navigate around moon. *GPS World*. <https://www.gpsworld.com/galileo-will-help-lunar-pathfinder-navigate-around-moon/>
- Delépaut, A., Giordano, P., Ventura-Traveset, J., Blonski, D., Schönfeldt, M., Schoonejans, P., Aziz, S., & Walker, R. (2020). Use of GNSS for lunar missions and plans for lunar in-orbit development. *Advances in Space Research*, 66(12), 2739–2756. <https://doi.org/10.1016/j.asr.2020.05.018>
- Donaldson, J. E., Parker, J. J. K., Moreau, M. C., Highsmith, D. E., & Martzen, P. D. (2020). Characterization of on-orbit GPS transmit antenna patterns for space users. *NAVIGATION: Journal of the Institute of Navigation*, 67(2), 411–438. <https://doi.org/10.1002/navi.361>
- DSN aperture fee calculator*. (2022). Retrieved November 22, 2022, from <https://dse.jpl.nasa.gov/ext/>
- DSN telecommunications link design handbook* (TMOD No. 810-005, Rev. E). (2018). Jet Propulsion Laboratory. Pasadena, CA. Retrieved November 8, 2022, from <http://deepspace.jpl.nasa.gov/dsndocs/810-005>
- Ely, T., Bhaskaran, S., Bradley, N., Lazio, T. J. W., & Martin-Mur, T. (2022). Comparison of deep space navigation using optical imaging, pulsar time-of-arrival tracking, and/or radiometric tracking. *The Journal of the Astronautical Sciences*, 69, 385–472. <https://doi.org/10.1007/s40295-021-00290-z>
- Enderle, W., Gini, F., Boomkamp, H., Parker, J. J., Ashman, B. W., Welch, B. W., Koch, M., & Sands, O. S. (2018). Space user visibility benefits of the multi-gnss space service volume: An internationally-coordinated, global and mission-specific analysis. *Proceedings of the 31st International Technical Meeting of The Satellite Division of the Institute of Navigation (ION GNSS+ 2018)*.
- Israel, D. J., Mauldin, K. D., Roberts, C. J., Mitchell, J. W., Pulkkinen, A. A., Cooper, L. V. D., Johnson, M. A., Christe, S. D., & Gramling, C. J. (2020). Lunanet: A flexible and extensible lunar exploration communications and navigation infrastructure. *2020 IEEE Aerospace Conference*, 1–14. <https://doi.org/10.1109/AERO47225.2020.9172509>
- Jet Propulsion Laboratory. (2023). *Horizons system*. Retrieved May 18, 2022, from <https://ssd.jpl.nasa.gov/horizons/>
- Johnston, M. D. (2020). Scheduling NASA's Deep Space Network: Priorities, preferences, and optimization. *ICAPS Scheduling and Planning Applications woRKshop (SPARK)*. <https://doi.org/2014/53269>
- Marquis, W. A., & Reigh, D. L. (2015). The GPS block IIR and IIR-M broadcast L-band antenna panel: Its pattern and performance. *NAVIGATION: Journal of the Institute of Navigation*, 62(4), 329–347. <https://doi.org/10.1002/navi.123>

- Montenbruck, O., Schmid, R., Mercier, F., Steigenberger, P., Noll, C., Fatkulin, R., Kogure, S., & Ganeshan, A. S. (2015). GNSS satellite geometry and attitude models. *Advances in Space Research*, 56(6), 1015–1029. <https://doi.org/10.1016/j.asr.2015.06.019>
- Musumeci, L., Dovis, F., Silva, J. S., da Silva, P. F., & Lopes, H. D. (2016). Design of a high sensitivity GNSS receiver for lunar missions. *Advances in Space Research*, 57(11), 2285–2313. <https://doi.org/10.1016/j.asr.2016.03.020>
- Parker, J. J. K., Bauer, F. H., Ashman, B. W., Miller, J. J., Enderle, W., & Blonski, D. (2018). Development of an interoperable GNSS space service volume. *Proceedings of the 31st International Technical Meeting of the Satellite Division of The Institute of Navigation (ION GNSS+ 2018)*, 1246–1256. <https://doi.org/10.33012/2018.15968>
- Parker, J. J. K., Dovis, F., Anderson, B., Ansalone, L., Ashman, B., Bauer, F. H., D'Amore, G., Facchinetti, C., Fantinato, S., Impresario, G., McKim, S. A., Miotti, E., Miller, J. J., Musmeci, M., Pozzobon, O., Schlenker, L., Tuozi, A., & Valencia, L. (2022). The Lunar GNSS Receiver Experiment (LuGRE). *Proceedings of the 2022 International Technical Meeting of The Institute of Navigation*, 420–437. <https://doi.org/10.33012/2022.18199>
- Petrick, D., Gill, N., Hassouneh, M., Stone, R., Winternitz, L., Thomas, L., Davis, M., Sparacino, P., & Flatley, T. (2015). Adapting the SpaceCube v2.0 data processing system for mission-unique application requirements. *2015 NASA/ESA Conference on Adaptive Hardware and Systems (AHS)*, 1–8. <https://doi.org/10.1109/AHS.2015.7231153>
- Psiaki, M. L. (2001). Block acquisition of weak GPS signals in a software receiver. *Proceedings of the 14th International Technical Meeting of the Satellite Division of The Institute of Navigation (ION GPS 2001)*, 2838–2850.
- Pultarova, T. (2022). This device will make GPS work on the moon. *Space.com*. <https://www.space.com/gps-navigation-at-the-moon-navimoon>
- Shehaj, E., Capuano, V., Botteron, C., Blunt, P., & Farine, P.-A. (2017). GPS based navigation performance analysis within and beyond the Space Service Volume for different transmitters' antenna patterns. *Aerospace*, 4(3), Article 44. <https://doi.org/10.3390/aerospace4030044>
- Small, J. L., Mann, L. M., Crenshaw, J. M., Gramling, C. J., Rosales, J. J., Winternitz, L. B., Hassouneh, M. A., Baker, D. A., Hur-Diaz, S., & Liounis, A. J. (2022). Lunar relay onboard navigation performance and effects on lander descent to surface. *Proceedings of the 2022 International Technical Meeting of The Institute of Navigation*, 587–601. <https://doi.org/10.33012/2022.18221>
- Space Communications and Navigation (SCaN) Mission Operations and Communications Services (MOCS)* (SCaN-MOCS-0001, Rev. 4). (2021). National Aeronautics and Space Administration. Retrieved November 21, 2022, from [https://explorers.larc.nasa.gov/2021APMIDEX/pdf\\_files/SCaN-MOCS-0001-Rev%20.4\\_Final.pdf](https://explorers.larc.nasa.gov/2021APMIDEX/pdf_files/SCaN-MOCS-0001-Rev%20.4_Final.pdf)
- Turan, E., Speretta, S., & Gill, E. (2022). Autonomous navigation for deep space small satellites: Scientific and technological advances. *Acta Astronautica*, 193, 56–74. <https://doi.org/10.1016/j.actaastro.2021.12.030>
- Ugazio, S., Peters, B. C., Croissant, K., Jenkins, G., McKnight, R., & van Graas, F. (2020). GNSS inter-system time-offset estimates and impact on high altitude SSV. *Proceedings of the 2020 International Technical Meeting of The Institute of Navigation*, 320–330. <https://doi.org/10.33012/2020.17146>
- United Nations Office for Outer Space Affairs. (2021). *The interoperable global navigation satellite systems space service volume* (2nd ed.). United Nations. <https://doi.org/10.18356/9789210000895>
- United States Coast Guard Navigation Center. (n.d.). *GPS technical references*. Retrieved August 19, 2023, from <https://www.navcen.uscg.gov/gps-technical-references>
- Wall, M. (2022). Success! nasa's tiny capstone probe arrives at the moon. *Space.com*. Retrieved November 30, 2022, from <https://www.space.com/nasa-capstone-cubesat-arrives-moon>
- Winternitz, L. B., Bamford, W. A., Long, A. C., & Hassouneh, M. (2019). GPS based autonomous navigation study for the Lunar Gateway [AAS 19-096]. *Proceedings of the 42nd AAS Rocky Mountain Section Guidance and Control Conference (AAS/GNC 2019)*.
- Winternitz, L. B., Bamford, W. A., & Price, S. R. (2017). New high-altitude GPS navigation results from the Magnetospheric Multiscale Spacecraft and simulations at lunar distances. *Proceedings of the 30th International Technical Meeting of the Satellite Division of The Institute of Navigation (ION GNSS+ 2017)*, 1114–1126. <https://doi.org/10.33012/2017.15367>
- Winternitz, L. B., Bamford, W. A., Price, S. R., Carpenter, J. R., Long, A. C., & Farahmand, M. (2017). Global positioning system navigation above 76,000 km for NASA's magnetospheric multiscale mission. *NAVIGATION: Journal of The Institute of Navigation*, 64(2), 289–300. <https://doi.org/10.1002/navi.198>

Winternitz, L. B., Moreau, M., Boegner, G. J., Jr., & Sirotzky, S. (2004). Navigator GPS receiver for fast acquisition and weak signal space applications. *Proceedings of the 17th International Technical Meeting of the Satellite Division of The Institute of Navigation (ION GNSS 2004)*, 1013–1026.